



# Desktop micromilled microfluidics

Ali Lashkaripour<sup>1,3</sup> · Ryan Silva<sup>2,3</sup> · Douglas Densmore<sup>2,3</sup> 

Received: 13 November 2017 / Accepted: 12 February 2018 / Published online: 26 February 2018  
© Springer-Verlag GmbH Germany, part of Springer Nature 2018

## Abstract

Micromilling is a proven method for prototyping microfluidic devices; however, high overhead costs, large machine footprints, an esoteric software stack, and nonstandard device bonding protocols may be hampering the widespread adoption of micromilling in the greater microfluidics community. This research exploits a free design-to-device software chain and uses it to explore the applicability of a new class of inexpensive, desktop micromills for fabricating microfluidic devices out of polycarbonate. We present an analysis framework for stratifying micromill's spatial accuracy and surface quality. Utilizing this we concluded milling geometries directly on the substrate is advantageous to making molds out of the substrate, in terms of accuracy and minimum feature size. Moreover, we proposed a general procedure to calculate feedrate and spindle-speed for any sub-millimeter endmill based on a recommended load percentage. We also established stepover is the major parameter in determining the surface quality rather than spindle-speed and feedrate, showing low-cost mills are able to deliver high-quality surface finishes. Ultimately, we clarified the suitability of low-cost micromills and a cost-efficient assembly method in the field of microfluidics by demonstrating rate- and size-controlled microfluidic droplet generation.

**Keywords** Microfluidics · Micromilling · Low cost · Microfabrication · Droplet microfluidics

## 1 Introduction

The field of microfluidics holds the promise of revolutionizing several fields, from biology and medicine to pharmaceutical and chemistry (Whitesides 2006; Squires and Quake 2005; Stone et al. 2004; Beebe et al. 2002). The microscale dimensions inherent to microfluidic channels reduce sample volume and error margins by several orders of magnitude when compared to macroscale liquid handling techniques such as pipetting by hand (Kintses et al. 2012). Additionally, elements of programmability (e.g., valving mechanisms, selection geometries, etc.) built into the microfluidic

device architecture can improve reaction time (Sackmann et al. 2014), experimental sensitivity (Dittrich and Schuille 2003), throughput (Thorsen et al. 2001), and accuracy (Luo et al. 2008). In light of these benefits, one would expect that microfluidic technology would be employed by a majority of laboratories in the life-sciences; however, reliance on lab-on-a-chip devices for conducting research remains very much the exception rather than the norm (Whitesides 2006). This dissonance can be attributed to a high barrier of entry inherent to microfluidic device fabrication, the traditional process for which resembles that of fabricating microelectronics. This process (i.e., photolithography in conjunction with soft-lithography) carries high equipment costs and infrastructure requirements that effectively limit the use of microfluidic devices to all but the most well-funded researchers (Sackmann et al. 2014).

While the traditional microfluidic device substrate, polydimethylsiloxane (PDMS), has been shown to be inexpensive (Brower et al. 2017), biocompatible (Ayoib et al. 2016), and optically transparent (Mogi et al. 2014), the process by which devices are realized (i.e., photolithography) is expensive and requires a host of specialized equipment and infrastructure such as a cleanroom, fume hood, mask aligner, spin coater, and plasma bonder. In addition, PDMS has some

---

**Electronic supplementary material** The online version of this article (<https://doi.org/10.1007/s10404-018-2048-2>) contains supplementary material, which is available to authorized users.

---

✉ Douglas Densmore  
doug@bu.edu

<sup>1</sup> Biomedical Engineering Department, Boston University, 44 Cummington Mall, Boston, MA 02215, USA

<sup>2</sup> Department of Electrical and Computer Engineering, Boston University, 8 Saint Mary's Street, Boston, MA 02215, USA

<sup>3</sup> Biological Design Center, 610 Commonwealth Avenue, Boston, MA 02215, USA

undesirable properties such as limited aspect ratio, weak mechanical properties, and swelling behavior when exposed to organic compounds (Mukhopadhyay 2007; Eddings et al. 2008; Guckenberger et al. 2015). On the other hand, micro-milling thermoplastics such as polycarbonate can provide a fast, semi-automated, and convenient alternative to photolithography (Yen et al. 2016; Chen et al. 2014). Thermoplastics have been shown to provide superior mechanical properties, biocompatibility, large aspect ratios, mass producibility, compatibility with organic compounds, and high working temperatures (Wu et al. 2009; Jankowski et al. 2011; Tsao and DeVoe 2009), making them ideal substitutes for PDMS. Recent advancements in inexpensive, desktop micromills, driven largely by the electronics hobbyist community and the desire to rapidly prototype printed circuit boards (PCB), present a new opportunity to remove many of the aforementioned barriers and expand the accessibility of microfluidic technologies. These computer numerical control (CNC) micromills can ablate a microfluidic geometry out of thermoplastics in minutes at a cost less than ten US dollar, thus creating an ideal prototyping platform for testing novel geometries and functionalities.

In here, we studied low-cost CNC mills suitability for microfluidics and presented a framework to characterize the performance of these machines through a set of standard tests, as shown in Fig. 1. Each test is made available to all through a text-based description of the test device in

OpenSCAD (an open-source CAD tool). The user can readily change the value of any parameter (e.g., depth of cut, feature size, spacing between features, endmill size, etc.) by editing the default value. In addition, a strategy for finding the milling settings (i.e., feedrate and spindle-speed) is introduced. Through this framework, three low-cost desktop CNC micromills (< \$3500) were tested: Othermill Pro, Othermill V2, and Carbide 3D’s Nomad 883. The performance of these machines was compared in terms of spatial accuracy and precision for positive features. Moreover, the minimum feature size, accuracy, and precision of milling a mold out of polycarbonate (positive features) and milling geometries directly on the substrate (negative features) were compared using the same CNC mill. Also, a generalized method is introduced to calculate the appropriate spindle-speed and feedrate for an endmill with a cutting diameter of 25–1000 μm. Furthermore, an inexpensive way of assembling polycarbonate microfluidic devices is introduced and characterized in terms of maximum bonding pressure. Afterward, surface quality of microchannels fabricated with a low-cost CNC mill is compared to that of a high-end CNC mill. Moreover, different parameters affecting surface roughness are studied. Finally, using the techniques presented in this study we designed, fabricated, assembled, and tested a microfluidic flow-focusing droplet generator, thus verifying the efficacy of the low-cost CNC mills in the field of microfluidics.

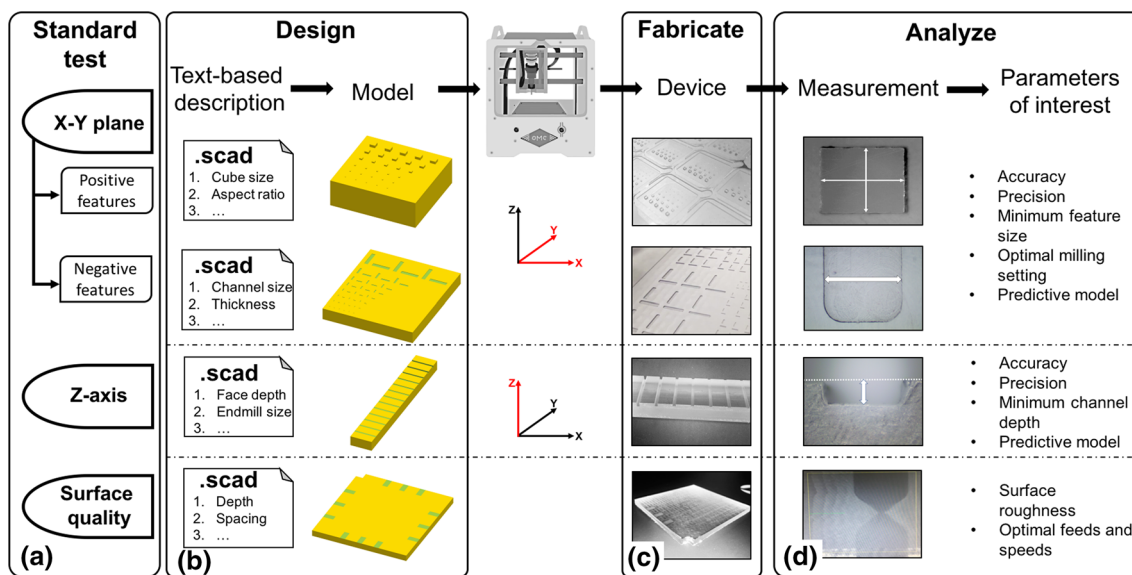


**Fig. 1** Set of standard tests proposed to characterize CNC micromills in terms of spatial accuracy and the surface quality of microchannels. **a** Three categories of standard tests, including spatial accuracy in X–Y plane both for positive and negative features (Sect. 2.5), spatial accuracy in Z-axis (Sect. 2.6) and surface roughness (Sect. 2.7). **b** Researchers can obtain CAD models of the standard tests using the text-based description of each test in OpenSCAD, also, they can

change any feature of the model, by adjusting the values of the variables (see Code S. 1–4). **c** Models are fabricated using any CNC mill. **d** Parameter of interest will be measured and compared to existing benchmarks, to characterize the performance of the CNC micromill. All the test devices can be found at: <https://github.com/CIDARLAB/milling-benchmarks/>

## 2 Materials and methods

### 2.1 Device substrate

Device geometries were milled directly into polycarbonate. While casting PDMS replicas of thermoplastic molds has been demonstrated (Yen et al. 2016), milling features directly into the thermoplastic substrate was preferred due to the reduction in assembly steps (Chen et al. 2014), tighter tolerances, and, as shown in Sect. 3.3, the ability to fabricate smaller features.

### 2.2 Software

Three levels of software are required to design and fabricate devices using a CNC micromill: a computer aided design (CAD) tool is used to create a solid model; computer aided manufacturing (CAM) software generates the commands that move the cutting tool; and control software to manage the connection between a computer and the micromill. Device designs were created using OpenSCAD, a free and open-source CAD tool that reads text files to generate solid models. The ability to describe a solid model solely using text is an important distinction between OpenSCAD and typical 3D modeling software packages (e.g., SolidWorks, AutoCAD, etc.), which often require geometries to be manually drawn. Modeling using textual descriptions opens the door for automatic generation of device designs using a high-level CAD workflow, such as (Huang and Densmore 2014). The CAD tool passes the solid model to CAM software where commands to manipulate the motion of the micromilling tool are generated. Autodesk Fusion 360 was used to generate these commands. Finally, each of the CNC mills has machine-specific control software. All of the software used in this study are free, but not necessarily open source.

### 2.3 Micromilling: feedrate and spindle-speed

The speed at which the cutting tool moves over the surface of the substrate (i.e., the feedrate) and the speed at which the cutting tool rotates while making contact with the substrate (i.e., spindle-speed) are crucial factors in enhancing the finish quality of the microchannel as well as increasing the lifetime of the cutting tool; each of these variables must be set while generating tool-paths using a CAM software. These parameters will change based on the diameter of the cutting tool, and the physical characteristics of the substrate. Determining values for these parameters is an inexact science, often involving trial-and-error

approach. To calculate appropriate feedrates and spindle-speeds manufacturers will often combine spindle-speed and cutting diameter into a single criterion known as surface speed (given in Eq. 1).

$$V = \pi \times \frac{D \times N}{1000} \quad (1)$$

where  $V$  is the surface speed (m/min),  $D$  is the cutting diameter (mm), and  $N$  is the spindle-speed (rpm). While surface speed provides useful guidance in determining feedrates and spindle-speeds for machining with larger diameter endmills (> 3 mm), the considerably smaller diameters inherent to micro-endmills, which can be as small as 5  $\mu\text{m}$ , may call for spindle-speeds that cannot be achieved by a desktop micromill. As a result the given range of surface speed values in handbooks and machining standards (Harper 2000; Solutions 2016) (60–150 m/min for milling on polycarbonate) no longer apply to micromilling. Interestingly, as our results show, surface speed may not be the most crucial factor in enhancing the lifetime of an endmill—the main effect for which being associated, rather, with load percentage (i.e., the thickness of the chip being sheared-off at each rotation of the endmill divided by the endmill's cutting diameter). A tolerable range of load percentages may be given for any endmill diameter. Considering load percentage, and by using Eq. 2 the feedrate is readily calculated. Therefore, in order to determine feedrate and spindle-speed for each endmill we studied the tolerable range of load percentage.

$$F = D \times N \times L \times T \quad (2)$$

where  $F$  is the feedrate (mm/min),  $D$  is the cutting diameter (mm),  $N$  is the spindle-speed (rpm),  $L$  is the load percentage (%), and  $T$  is the number of flutes. In order to determine if a given spindle-speed and feedrate is correct and will not damage the endmill or the work-piece, a microchannel was milled with length, width, and depth measuring  $200 \times D$ ,  $4 \times D$ , and  $1.5 \times D$ , respectively, where  $D$  is the endmill's cutting diameter. After each milling session the endmill was inspected for damage. In here, no damage is the determinant of a successful milling session and an acceptable spindle-speed and feedrate.

### 2.4 Bonding

To assemble the microfluidic device, flow layer and control layer are sealed through a thin (100–500  $\mu\text{m}$  depending on a specific application and valve size) PDMS membrane in between and are held together using binder clips which frees researcher from the trouble of thermal bonding. The PDMS layer is made through an established method (Silva et al. 2016). It should be mentioned that the PDMS layer keeps the chip sealed through Van Der Waals forces which is further reinforced with binder clips (see Fig. S. 2.).

## 2.5 X–Y plane characterization

In order to compare the accuracy and precision of positive features (making molds out of polycarbonate) and negative features (milling the microchannels directly on polycarbonate), we designed and fabricated a set of devices as explained below. To measure the feature's size, we used a calibrated microscope and ImageJ as the image processing tool.

### 2.5.1 Positive features

To study the spatial accuracy of positive features, a set of cuboids were milled, with an aspect ratio of 0.5. The size of these squares is varied from 1000 to 100  $\mu\text{m}$ . In order to assess the precision of the micromills, each chip includes five technical replicates of the cuboids. To account for experimental variations, four experimental replicates of this chip are fabricated. It should be mentioned, all these experiments were carried out with unused 793.7  $\mu\text{m}$  (1/32") endmills. In order to compare the accuracy and the precision of different machines, these experiments were carried out for all the mills.

### 2.5.2 Negative features

To investigate the spatial accuracy of negative features, we milled microchannels both with horizontal and vertical orientation. The width of these microchannels was chosen to be  $1 \times D$ ,  $1.5 \times D$ , and  $2 \times D$  ( $D$  = cutting diameter of endmill). We have used 793.7, 396.8, 254, 200, 150, 100, and 75  $\mu\text{m}$  endmills. Therefore, the minimum channel width would be 75  $\mu\text{m}$  ( $1 \times 75 \mu\text{m}$ ) and the maximum would be 1587.4  $\mu\text{m}$  ( $2 \times 793.7 \mu\text{m}$ ). The microchannel's width is measured to determine the accuracy and precision. The channels with vertical orientation represent X-axis, and the horizontally oriented channels represent Y-axis.

## 2.6 Z-axis characterization

A substantial feature of microfluidic devices is the channel depth, since the channel resistance varies with channel depth to the power of three (as given in Eq. 4) and small variations in channel depth could lead to significant alteration in flow field (Aubin et al. 2009). To characterize the accuracy of desktop mills in Z-axis, we milled channels with a constant width and decreasing depth. We varied channel depth from 1000 to 40  $\mu\text{m}$ . All the measurements in Z-axis were carried out using a calibrated microscope.

## 2.7 Surface roughness

An important characteristic of microchannels is its surface roughness, which can affect biocompatibility, transparency,

and apparent viscosity (Prentner et al. 2010). To compare low-cost mills to high-end machines, we replicated Chen et al. (2014) experiment and milled a 6 mm  $\times$  3 mm rectangle. The feedrates and spindle-speeds were varied according to Chen et al. experiment, the depth of cut was kept constant at 15  $\mu\text{m}$ , due to the insignificance of depth of cut for depths of cut up to 300% of endmills cutting diameter (Guckenberger et al. 2015). The features were milled with a 254  $\mu\text{m}$  endmill, once while keeping a 20% stepover (Chen et al. experiment) and once at 5%, to study the effect of stepover on surface quality. Additionally, to further clarify the effect of stepover on surface roughness and machining time, we varied the stepover from 5 to 30%, while keeping the feedrate at 600 mm/min and the spindle-speed at 15,000 rpm, using two different endmill sizes (i.e., 254 and 397  $\mu\text{m}$ ). All the measurements have been carried out using Alpha-Step 500 Profiler, the scan length was set at 1 mm, scan speed was set at 0.2 mm/s, and the stylus force was set at 19.9 mg.

## 2.8 Microfluidic flow-focusing droplet generation

Droplet microfluidics advantages over continuous-flow microfluidics, such as accurate volume control, high throughput, high sensitivity, and low sample consumption leads to faster, cheaper, and more accurate results (Thorsen et al. 2001; Lashkaripour et al. 2015). Droplet generation can be achieved by flowing an aqueous and a non-aqueous fluid, through a microfluidic geometry (Tirandazi and Hidrovo 2017; Lashkaripour et al. 2018) as shown in Fig. 2. To demonstrate the efficacy of desktop mills and low-cost bonding in fabricating microfluidic devices and study the importance of minimum feature size in microfluidics, we made multiple flow-focusing droplet generator with varying orifice widths (i.e., minimum feature size) from 75 to 397  $\mu\text{m}$ . For the aqueous phase we used DI water and added Allura Red for better visualization; for the non-aqueous phase, we used mineral oil with an addition of Span 80 surfactant to enhance droplet stability. More information on droplet generation is given in Table 1.

## 3 Results

### 3.1 Feedrate and spindle-speed

We found out that the recommended surface speed of 60–150 m/min for polycarbonate does not apply to micro-milling; due to significant size reduction, most machines cannot spin the endmill fast enough to reach the recommended surface speeds (see Sect. 2.3). In fact, for a 254  $\mu\text{m}$  endmill, we varied surface speed from 6.39 (minimum spindle-speed of 8000 rpm) to 20.76 m/min (maximum spindle-speed of 26,000 rpm), using Eq. (3) this means we



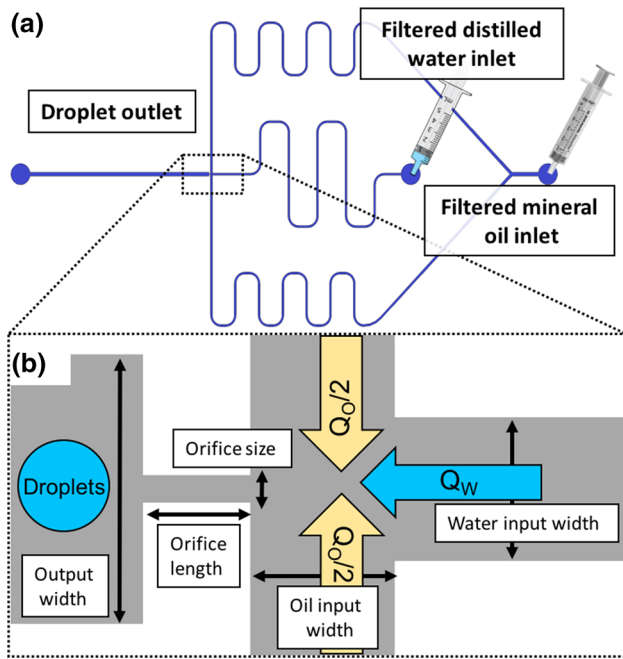


**Fig. 2** Flow-focusing droplet generation as a proof of concept of the applicability of low-cost fabrication and bonding method in microfluidics. **a** Schematic of the microfluidic device used to generate water-in-oil droplets. **b** Zoomed-in view of the flow-focusing geometry and its parameters (given in Table 1)

**Table 1** Geometric parameters and fluid properties used to achieve microfluidic flow-focusing droplet generation

Geometry		Fluid properties	
Orifice size	75–397	Aqueous phase	DI water
Orifice length	300	Non-aqueous phase	Mineral oil
Water input width	400	Oil viscosity	77.8 mPa.s
Oil input width	400	Oil density	0.857 kg/m <sup>3</sup>
Output width	750	Surfactant	3% span 80
Channel depth	300	Aqueous phase dye	Allura red

varied feedrate from 162.5 to 528.3 mm/min, while keeping the load percentage constant at 4%, and milled successfully. Moreover, note that this range is well below the recommended range of 60–150 m/min given in handbooks (Solutions 2016). We have also carried out the same experiment for a 396.8 μm endmill, we varied the surface speed from 9.98 to 32.43 m/min (i.e., feedrate: 254–825.5 mm/min) and milled successfully. Since we clarified surface speed is not a key parameter, we hypothesized that load percentage is the crucial factor for successful milling. Therefore, to confirm this, we aimed to find the range of tolerable load percentage for a number of endmills. As shown in Fig. 3, we examined six different endmills and increased the load percentage with 1% steps, to measure the maximum tolerable load

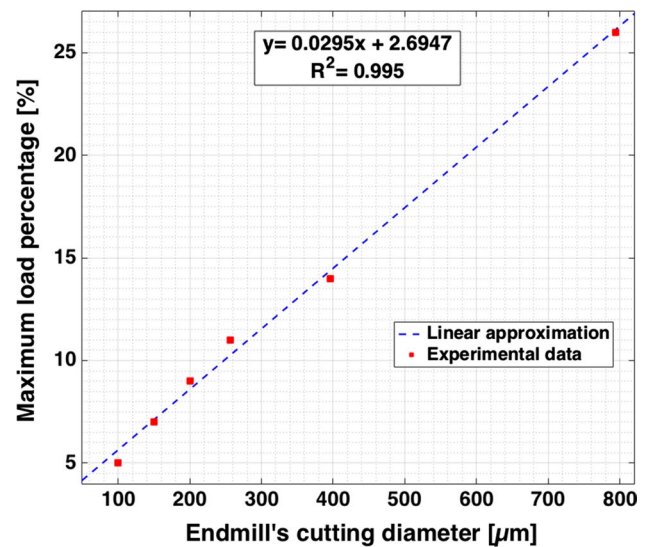


**Fig. 3** Variation of load percentage with endmill's cutting diameter shows a linear relation. This linear equation can be used to approximate the maximum tolerable load percentage for any sub-millimeter endmill size, freeing researchers from trial and error. By using this equation we predicted (not verified) the load percentage suitable for a 50 and a 25 μm endmill

**Table 2** Recommended milling setting based on tolerable load percentage for different endmill sizes

Endmill diameter (μm)	Spindle-speed (rpm)	Feedrate (mm/min)	Plunge rate (mm/min)	Step-down (mm)	Load (%)
794	12,000	900	40	0.25	6
397	12,000	500	36	0.25	5.2
254	14,000	300	16	0.15	4
200	15,000	240	10	0.1	4
150	15,500	186	7	0.07	4
100	16,000	96	4	0.04	3
75	17,000	76.5	2	0.02	3
50	18,000	36	1	0.01	2
25	19,000	8	0.5	0.01	1

These values are only valid for micromilling on a polycarbonate substrate

percentage. We observed a linear dependency of maximum load percentage on endmill's cutting diameter, as shown in Fig. 3. Therefore, we recommended a safe load percentage for each endmill size, alongside spindle-speed, feedrate, plunge rate, and step-down as given in Table 2. It should be mentioned, since the load percentage is the crucial factor to a successful milling session, researchers do not have to follow the exact values given in Table 2; because some desktop mills cannot deliver the recommended spindle-speeds. One can easily follow the procedure shown in Fig. 4 to find the milling setting for any sub-millimeter endmill size.

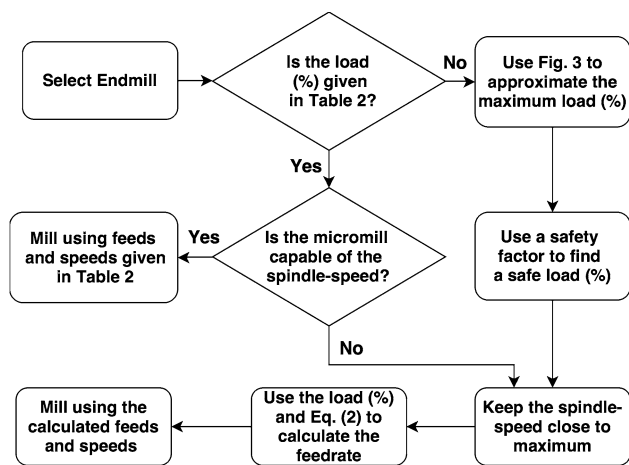


**Fig. 4** Procedure proposed to find feedrate and spindle-speed for micromilling on polycarbonate using any sub-millimeter endmill. This eliminates the need for costly trial and errors to find the milling setting

## 3.2 Bonding pressure

In order to test the maximum pressure tolerable with the proposed bonding method, we milled a 80-mm-long channel with a  $400\ \mu\text{m} \times 400\ \mu\text{m}$  cross section and flowed 350 NF mineral oil with a viscosity of 77.8 mPa.s through the channel. We flowed 17 mL/h of mineral oil without sealing issues. Using Eq. (3) to calculate the pressure generated in the channel, we concluded the bonding pressure of our assembly method is 5.3 PSI (neglecting the resistance of ports and tubes).

$$\Delta P = R_{\text{fluid}} \times Q \quad (3)$$

where  $\Delta P$  is the pressure drop (Pa),  $R$  is the resistance of the channel, given in Eq. (4), and  $Q$  is the flow rate ( $\text{m}^3/\text{s}$ ). It should be noted that Eq. (4) holds true only for microchannels where  $2 \times H > W$  (Bahrami et al. 2006).

$$R = 32 \times \frac{\mu L}{WH^3} \quad (4)$$

where  $\mu$  is the fluid viscosity (Pa.s),  $L$ ,  $W$ , and  $H$  are the channel length, width, and depth (m), respectively. Researchers with certain applications that require a higher bonding pressure can utilize thermal bonding as described in the literature (Tsao and DeVoe 2009; Silva et al. 2017). In here, for the sake of keeping the total equipment cost and the fabrication time at a minimum we only characterized the bonding method presented in Sect. 2.4.

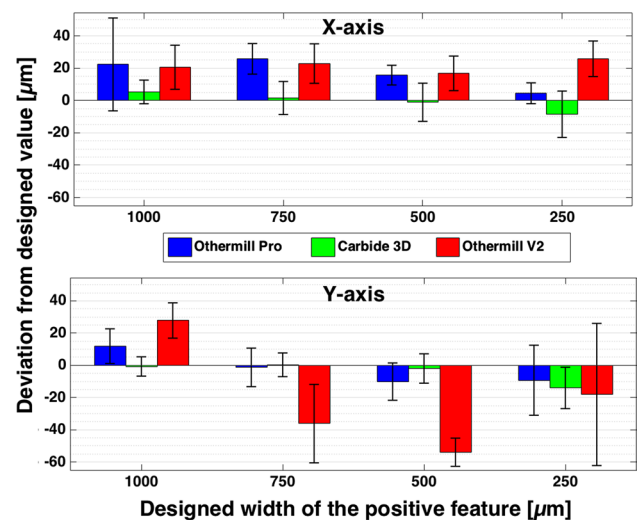


**Fig. 5** Although, Carbide 3D shows great accuracy in X-Y plane in comparison with the Othermills, all the mills failed to accurately mill a positive feature smaller than  $250\ \mu\text{m}$ . The total length of the error bars represents two standard deviations for  $N = 20$ . Positive values represent an under-cut, and negative values represent an over-cut

## 3.3 X-Y plane characterization

### 3.3.1 Positive features

For positive features we observed that they were damaged or not square shaped, for dimensions smaller than  $250\ \mu\text{m}$  (keeping aspect ratio at 0.5). This undermines the reliability of low-cost mills in fabricating polycarbonate molds to make PDMS-based devices (due to their lower accuracy in comparison with high-end mills). However, for dimensions equal/larger than  $250\ \mu\text{m}$  the maximum of the average deviations from the designed values was 8.5 (14.0), 25.7 (11.9) and 25.8 (53.9)  $\mu\text{m}$  for Carbide 3D, Othermill Pro, and Othermill V2, respectively, in X-axis (Y-axis). Moreover, we assumed the precision of the mills to be three times the value of the maximum standard deviation. Based on this, we calculated the precisions in X-axis (Y-axis) to be 42.9 (38.4), 86.1 (65.1), and 40.8 (132.3)  $\mu\text{m}$ , for Carbide 3D, Othermill Pro, and Othermill V2, respectively. Figure 5 shows all the data in a single graph. It should be mentioned researchers can account for these inaccuracies by using models such linear regressions. As shown in Fig. 5, the machines show different spatial accuracies in X-axis in comparison with Y-axis. This is due the fact that these machines use different motors for each axis which results in different spatial accuracies. This different spatial accuracy behaviors in each axis can also be observed in high-end micromills (Chen et al. 2014).

### 3.3.2 Negative features

Unlike 250 μm minimum dimension in positive features, for negative features we were able to mill features as small as 75 μm. We were not able to make smaller features because endmills smaller than 75 μm (i.e., 50 and 25 μm) break during locating the tool via the software provided by the manufacturer. However, these small endmills still can be located through manual manipulation of the G-code that is sent to the machine. All the features that were milled were 2×, 1.5×, or equal to the endmill’s cutting diameter. If the same data point could be reached using two different endmills (e.g., 200 μm : 2 × 100 μm or 1 × 200 μm), we presented the data for the smallest multiple (i.e., 1 × 200 μm), to show the best accuracies and precisions that can be reached using desktop mills. Therefore, we grouped the data shown in Fig. 6 in three categories (2×, 1.5×, and 1× endmill’s cutting diameter). As shown in Fig. 6, milling negative features will result in tighter tolerances and decreases the minimum features size considerably (limited to smallest endmill available) in comparison with positive features. Interestingly, when only considering the data points were the width of the channel was equal to the endmill’s cutting diameter, the maximum deviations were significantly reduced, as given in Table 3.

### 3.4 Z-axis characterization

Through the method described in Sect. 2.6, the largest average deviation from designed channel depth for 10 devices

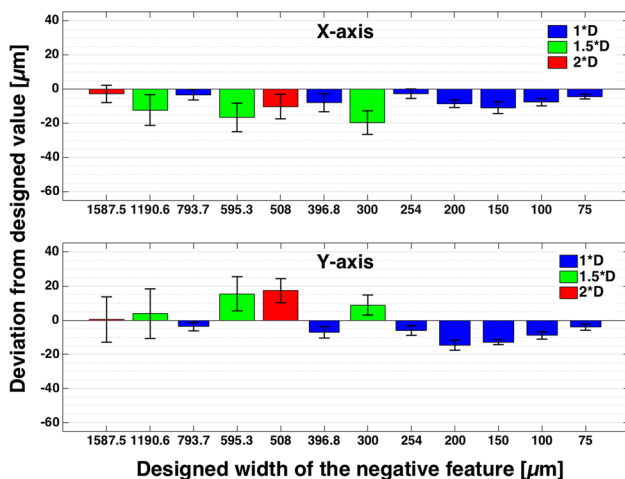


**Fig. 6** Milling negative features is favorable to milling positive features in terms of accuracy, precision, and minimum feature size. It can be seen, although none of the mills were able to fabricate positive features smaller than 250 μm (see Fig. 5), Othermill Pro can fabricate negative features as small as 75 μm accurately. The total length of the error bars represents two standard deviations for  $N = 9$ . Positive values represent an under-cut, and negative values represent an over-cut

was 5.9, 10.4, and 9.7 μm for Carbide 3D, Othermill Pro, and Othermill V2, respectively. In addition, the precision ( $3 \times SD$ ) was found to be 35.1, 61.3, and 26.4 μm, for Carbide 3D, Othermill Pro, and Othermill V2, respectively. Figure 7 shows all the data in a single graph. To compensate for the inaccuracies in the Z-axis, we recommend researchers to model the data points to find a trend in their machines, such as the models presented in Fig. 7b.

### 3.5 Surface roughness

It is expected that increasing spindle-speed and decreasing feedrate decreases the surface roughness (Guckenberger

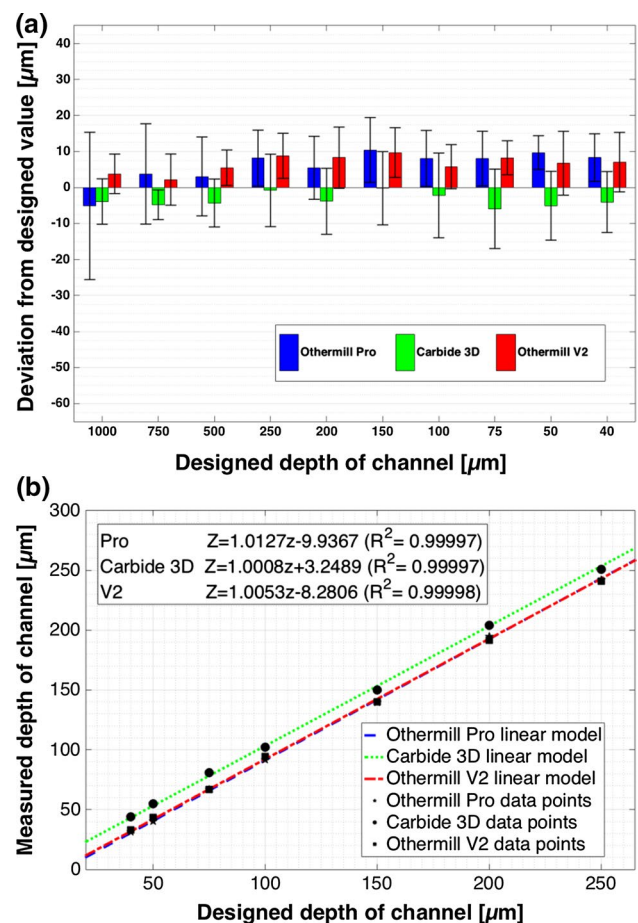


**Fig. 7** Comparison of the Z-axis accuracy for three different CNC mills. **a** All the mills show almost a similar performance in Z-axis in terms of spacial accuracy with some amount of deviations from the designed values. The total length of the error bars represents two standard deviations for  $N = 10$ . (Positive values represent an under-cut, and negative values represent an over-cut.) **b** Building linear models based on these data points shows that these deviations could be easily accounted for by characterizing the performance of a CNC mill and building a model based on any method such as the linear regression model given here. Keeping the almost linear behavior of these mills in mind one can approximate the actual depth of a channel for any designed value

**Table 3** Comparison of positive and negative features in terms of X–Y plane performance using Othermill Pro

Parameter	Positive features (μm)	Negative features (μm)
Minimum feature size	250	75
Worst X-axis accuracy	25.7	19.6
Worst Y-axis accuracy	11.9	17.3
Worst X-axis precision	86.1	26.8
Worst Y-axis precision	65.1	39.9
Max. X-axis deviation	60.9	36.5
Max. Y-axis deviation	52.8	36.4
Max. X-axis dev. for features equal to endmill diameter	60.9	22.1
Max. Y-axis dev. for features equal to endmill diameter	52.8	20.7

This illustrates the effectiveness of milling negative features in microfluidics while using a low-cost CNC mill

et al. 2015; Chen et al. 2014). However, data presented in those studies were inconclusive. On the other hand, some studies suggest there is an optimal value for feedrate that results in the smoothest surface (Lee and Dornfeld 2004). Similarly, we observed there are optimal values for

spindle-speed and feedrate and researchers should evaluate their mills to find the spindle-speed and feedrate that results in the minimum surface roughness, as shown in Fig. 8b. In the mentioned studies the stepover was kept constant. Interestingly, we found stepover to be crucial to surface finish. When replicating Chen et al. experiment (Chen et al. 2014), we measured our surface quality to be worse than that of a high-end mill, which is reasonable because desktop micromills, due to their small size, are more prone to vibrations induced by their motors. However, decreasing the stepover from 20% (Fig. 8b) to 5% (Fig. 8c), resulted in a surface much smoother and even smoother than most of Chen et al. experiments carried out at 20% stepover. Moreover, with a stepover of 5% we observed that the roughness is less dependent on feedrate and spindle-speed, as shown in Fig. 8c. While keeping the stepover at 5% we reached a minimum surface roughness of  $R_a = 0.205 \pm 0.029 \mu\text{m}$ . For a constant feedrate and spindle-speed, decreasing stepover results in an increase in machining time as shown in Fig. 9a. Also, as shown in Fig. 9b, there is a trade-off between machining time and surface roughness as increasing stepover results in a reduced machining time and a greater surface roughness. Moreover, as demonstrated in Fig. 9b a smaller endmill generally results in a lower surface roughness.

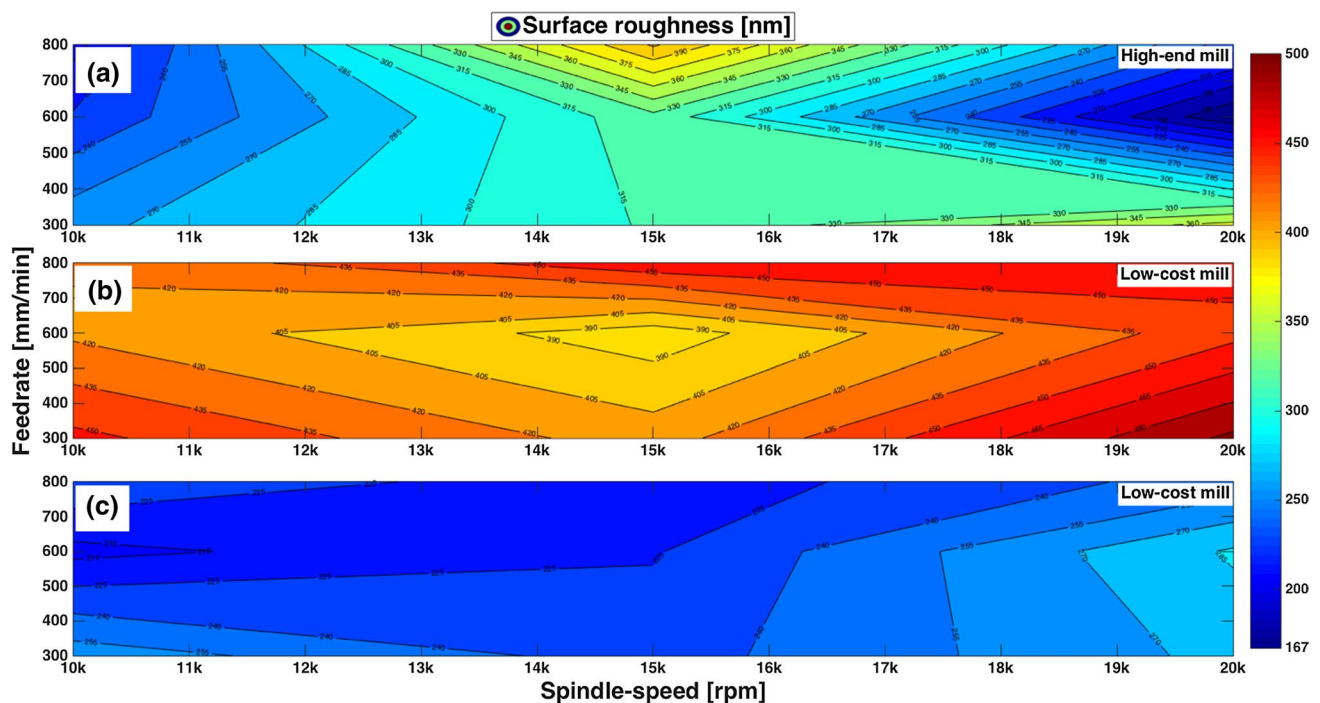


**Fig. 8** Rather than feedrate and spindle-speed, stepover is the most important factor in defining surface quality. Therefore, desktop micromills can deliver high-quality surface finishes. Effect of spindle-speed, feedrate, and stepover on surface roughness is shown for a 15 μm deep microchannel using **a** high-end CNC mill at 20% ste-

pover (Chen et al. 2014). **b** Low-cost CNC mill at 20% stepover. **c** Low-cost CNC mill at 5% stepover. The data shown in **(b)** and **(c)** are the average of 9 measurements (3 microchannels measured at 3 points). Each contour represents a 15-nm variation in surface roughness



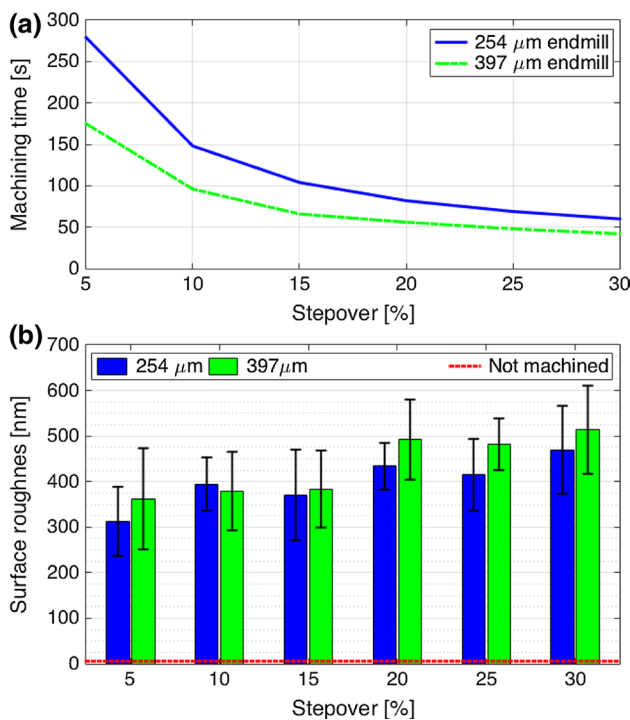


**Fig. 9** Stepper and endmill size are crucial to **a** machining time and **b** surface roughness. Decreasing endmill size and stepper results in a longer machining time and generally a smoother surface. In this experiment, a rectangle with a size of 6 mm × 3 mm for a depth of cut of 15 μm was milled while keeping the feedrate at 600 mm/min and spindle-speed at 15,000 rpm. The surface roughness of polycarbonate before machining is 6.49 ± 4.02 nm. The total length of the error bars represents two standard deviations for N = 4

### 3.6 Microfluidic flow-focusing droplet generation

As a proof of the reliability of the aforementioned fabrication and bonding method, we fabricated a flow-focusing microfluidic droplet generator with a 75 μm orifice width. We have tested the device at two flow rate ratios, while keeping the water flow rate constant at 0.3 mL/h. Snapshots of the experiments are shown for flow rate ratio of  $\phi = 3.33$  and  $\phi = 33.33$  in Fig. 10. At low flow rate ratios we generated a stream of droplets with high aqueous phase to non-aqueous phase ratio, at a rate of 10 droplet per second. Moreover, at high flow rate ratio we generated monodispersed droplets of ≈ 0.2 nL in volume at a rate of 80 droplets per second. Interestingly, due to the hydrophobic nature polycarbonate, it does not require any surface modifications for droplet generation, unlike PDMS-based devices (Barbier et al. 2006). Finally, as shown in Fig. 11, to demonstrate the importance of the minimum feature size in microfluidic droplet generation, we fabricated three droplet generators with the geometry stated in Table 1, except the orifice size that was set to be 75, 254, and 397 μm. The flow rate of oil and water was kept constant at 5.5 and 0.36 mL/h, respectively. We observe

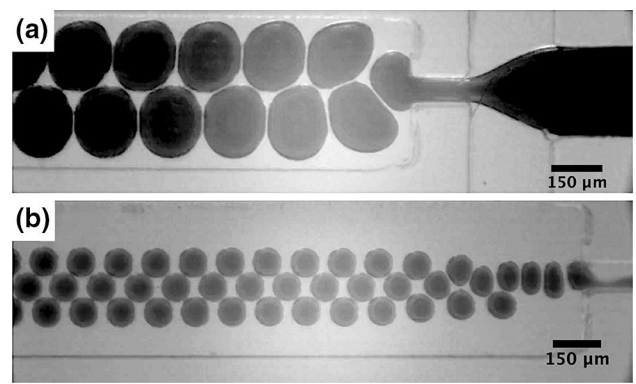


**Fig. 10** Microfluidic droplet generation, which demonstrates the effectiveness of low-cost mills and inexpensive bonding in microfluidics. Flow rate of water was kept at 0.3 mL/h, and flow rate of mineral oil was varied from **a** 1 mL/h to **b** 10 mL/h (generation rate of 80 Hz)

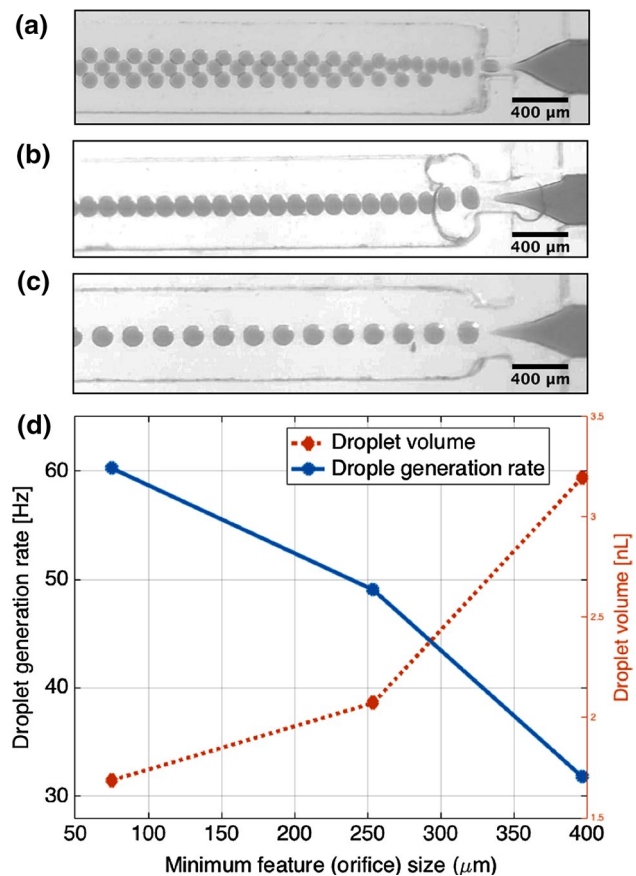


**Fig. 11** Minimum feature size (i.e., orifice width) has a significant effect on both generation rate and droplet volume in a microfluidic droplet generator. Decreasing minimum feature size while keeping the oil and water flow rate constant (5.5 and 0.36 mL/h, respectively) results in an increased droplet generation rate and a reduced droplet volume. **a** An orifice size of 75 μm. **b** An orifice size of 254 μm. **c** An orifice size of 397 μm. **d** Variation of droplet generation rate and droplet volume with the orifice size

that changing the orifice size from 75 to 397  $\mu\text{m}$  results in a reduction in the generation rate from 60 to 30 Hz. Also, the droplet volume increases from 1.7 to 3.2 nL.

## 4 Discussion

We have proposed a framework to evaluate the performance of any micromill in terms of spatial accuracy, minimum feature size, and surface quality. In addition to this, we characterized a fast and low-cost bonding method to assemble microfluidic devices in an efficient manner. Finally, to bring all the findings of this study together, we designed a microfluidic droplet generator, that was fabricated as a negative feature, using our recommended feedrate and spindle-speed, and assembled using the low-cost bonding method. As a result, we established that desktop micromills are low-cost and efficient machines capable of introducing a new-era of accessible-to-all microfluidics. In this section, we elaborate more on the findings of this study and we compare low-cost micromilling to common microfabrication methods (i.e., photolithography and high-end micromilling) in terms of equipment cost, cost per device, spatial accuracy, surface roughness, and the required infrastructure.

### 4.1 Feeds and speeds

An important aspect of micromilling microfluidic devices on polycarbonate is the machine's setting, having these numbers mistaken could result in a long fabrication time, low-quality surface finish, or even a broken endmill which can cost up to hundreds of US dollars. We have found that machining features, specifically in thermoplastics using endmills with a diameter of less than 1000  $\mu\text{m}$  create unique challenges. Surface speed of 60–150 m/min recommended for milling on polycarbonate is no longer achievable due to the significant reduction in endmill's cutting diameter and limited spindle-speed of current low-cost mills. In here, we introduced load percentage as the crucial factor to a successful milling. Meaning that feedrate and spindle-speed can take a wide range of values as long as the load percentage is within the tolerable range. We have shown this, with a set of different endmills, for instance while using a 254  $\mu\text{m}$  endmill we milled varying the feedrate from 162.5 to 528.3 mm/min and increasing the spindle-speed from 8000 to 26,000. As a result, a mill that can deliver high spindle-speeds is capable of milling at faster feedrates while keeping the load percentage constant, hence not breaking the endmill. This clarifies the significance of maximum spindle-speed of a mill in rapid prototyping and reducing fabrication time. On the other hand, load percentage affects tool wearing, too much and too little load percentage can quicken tool wear (Pansare and Sharma 2013). Increased load percentages can result in

a broken endmill, and reduced load percentages result in a phenomenon called rubbing which results in a rough surface and an increased tool wear (Mian et al. 2011). Tool wearing is less crucial in milling polycarbonate due the softness of the material (Chen et al. 2014). Nonetheless, a worn-out tool results in an elevated cutting temperature which can have adverse effects on surface quality. Therefore, we suggest researchers to visually inspect endmills on a regular basis and replace the worn-out endmills.

### 4.2 Spatial accuracy and minimum feature size

We characterized three desktop mills, providing a set of benchmarks for future studies. While characterizing the spatial accuracy of the positive features, although we set our minimum dimensions to be 100  $\mu\text{m}$ , we observed that the mills were not able to properly fabricate cuboids smaller than 250  $\mu\text{m}$  (see Fig. S. 8). Therefore, we only presented the data for dimensions down to 250  $\mu\text{m}$ . On the other hand, while milling the negative features the minimum feature size is dependent on endmill's diameter. Because Othermill Pro locates the endmill upon the contact of the tool and the mill's bed, and  $\leq 50 \mu\text{m}$  endmills break upon contact (see Fig. S. 8), we were unable to use endmills smaller than 75  $\mu\text{m}$ . Therefore, the minimum feature size for negative features will be 75  $\mu\text{m}$ , which is still significantly smaller than that of the positive features. In addition to this, we observed much tighter tolerances while milling negative features, specially when the channel width is equal to the endmill's cutting diameter. These machines have limited spatial resolution (25  $\mu\text{m}$  for Othermill Pro and V2, and 13  $\mu\text{m}$  for Carbide 3D Nomad 833); therefore, the best accuracies can be achieved when the machine resolution is not introduced to the total error. Through this, the source of error left will be tool deflection, machine's vibrations, and endmill cutting diameter's tolerances.

### 4.3 Bonding pressure

To make any microfluidic geometry functional, it should be sealed and assembled. This is usually carried out through thermal bonding which could result in deformation of features with high aspect ratio (Ogonczyk et al. 2010). Therefore, we have introduced a fast and cost-efficient assembly method of microfluidic devices, which can withstand up to  $\sim 5$  PSI of pressure before the seal breaks. Although, the maximum bonding pressure is much less than 50 PSI tolerated in PDMS-glass bonded devices, still the proposed assembly method, provides enough bonding pressure for a wide variety of microfluidic applications, where the maximum pressure is lower than 5 PSI (Rasouli et al. 2015; Ward et al. 2005; Kang et al. 2008). We observed proper sealing up to 24 h while flowing an aqueous solution (i.e., DI

water) and up to 8 h while using a non-aqueous solution (i.e., mineral oil). Generally, a thicker layer of PDMS will result in a better sealing by increasing the pressure enforced by the binder clips; however, valve actuation requires a greater vacuum pressure while using thicker PDMS.

#### 4.4 Surface quality

Finishing quality of a microchannel is directly linked to its surface roughness; in addition, surface roughness plays a major role in the biocompatibility of a microfluidic device (Guckenberger et al. 2015). Therefore, for most applications a smoother surface is more desirable. Studies usually consider the effect of spindle-speed and feedrate on surface roughness (Guckenberger et al. 2015; Chen et al. 2014). These studies suggest that there are optimal points that should be found experimentally through a conclusive design of experiment. These studies were carried out while keeping the stepover constant. We found out that decreasing the stepover results in a significant reduction of surface roughness, making it the major parameter determining the surface finish quality. However, there is a trade-off between machining time and surface roughness as increasing stepover decreases machining time but results in a rougher surface. Therefore, researchers can choose a stepover depending on their application and priorities. Increasing surface roughness also increases light absorbance and reduces transparency of microchannels, which can be mitigated through sanding and/or vapor polishing as previously demonstrated (Yen et al. 2016).

#### 4.5 Comparison of desktop micromilling to common microfabrication methods

Cost of microfabrication is a major road-block to the widespread use of microfluidic devices. In Table 4 we compared photolithography, high-end micromilling, and low-cost micromilling, in terms of equipment cost, cost of each device, required infrastructure and performance metrics. For photolithography we assumed out-sourcing the photomask then using standard photolithography alongside soft-lithography to fabricate a microfluidic device (see Sect. S. 8. 1. for more details and pricing breakdown). Cost of endmills was estimated for high-end milling by a total price of a set of endmills from 5  $\mu\text{m}$  to 3.175 mm (see Sect. S. 8. 2.), and for low-cost endmills we assumed a set from 75  $\mu\text{m}$  to 3.175 mm (see Sect. S. 8. 3.). For high-end and low-cost micromilling we assumed the same assembly and bonding method as the one introduced in Sect. 3.2. One can use other bonding methods that can deliver higher bonding pressures; however, the total cost of equipment and the cost per device will increase. For surface quality we used the data from (Tang et al. 2015) for PDMS, the

data presented by (Chen et al. 2014) for high-end micromilling and the data provided in our study for low-cost micromilling. For minimum feature size, common mask writers deliver at least a  $\pm 1 \mu\text{m}$  resolution; therefore, the minimum feature size for photolithography is considered to be  $\leq 1 \mu\text{m}$ . For high-end micromilling the smallest feature size is limited by the smallest endmill available, which is 5  $\mu\text{m}$  (see Sect. S. 8. 2.). For low-cost micromilling, although we showed a 75  $\mu\text{m}$  minimum feature size, one can locate smaller endmills without breaking it through manipulation of the G-code being sent to the machine, thus, achieving even smaller minimum feature sizes. The total cost of consumables for each device is assumed to be the cost of a single device, neglecting salaries, maintenance costs, etc. Replication of PDMS-based devices becomes significantly cheaper than making new designs due to the high cost of a photomask; however, even in this case each device is significantly more expensive than micromilling microfluidic devices. Unlike photolithography, micromilling does not require any infrastructures such as cleanroom, fume hood, vacuum line, and tank storage. As a result, although desktop micromills have a limited minimum feature size and surface roughness, they are ideal tools for rapid prototyping of microfluidic devices for most of the applications, due to the significant reduction in fabrication time, cost, and the required equipment and infrastructure.

## 5 Conclusion

We provided a framework to characterize the performance of desktop micromills. We showed the efficacy of low-cost mills and a time- and cost-effective assembly method in fabricating microfluidic devices. Through this framework we achieved a minimum feature size of 75  $\mu\text{m}$  and a maximum bonding pressure of 5.3 PSI. Also, it was illustrated ablating geometries directly on polycarbonate results in a better accuracy, while reducing the minimum feature size significantly. Moreover, by identifying load percentage as the crucial factor to a successful milling, we concluded that milling can be performed much faster with the new generation of micromills that support high spindle-speeds. Additionally, we showed stepover is the crucial parameter in determining the surface quality, based on this we fabricated a microchannel with a surface roughness of  $R_a = 0.205 \mu\text{m}$ . Finally, we used the low-cost framework to fabricate a microfluidic droplet generator that produced 0.2 nL droplets at a rate of 80 Hz. Therefore, we clarified low-cost desktop micromills are capable of becoming the ideal (fastest and least expensive) fabrication technique for prototyping microfluidic devices.

**Table 4** Comparison of low-cost micromilling to photolithography and high-end micromilling, in terms of cost equipment and consumables, required infrastructure and performance metrics

Items	Photolithography	High-end milling	Low-cost milling
<b>Equipment</b>			
Micromill	N.R.*	\$15.5–220 K	\$2.5–3.2 K
Endmill set	N.R.	~ \$1 K	~ \$0.5 K
Mask aligner	~ \$65 K	N.R.	N.R.
Plasma bonder	~ \$6.6 K	N.R.	N.R.
Spin coater	~ \$4 K	N.R.	N.R.
Stereomicroscope	~ \$1.5 K	N.R.	N.R.
Incubator	~ \$0.3 K	N.R.	N.R.
Desiccator	~ \$0.1 K	~ \$0.1 K	~ \$0.1 K
Toaster oven	N.R.	~ \$50	~ \$50
<b>Consumables</b>			
Photomask	~ \$95–400	N.R.	N.R.
Photoresist	~ \$40	N.R.	N.R.
PDMS	~ \$10–30***	≤ \$5	≤ \$5
Developer	~ \$20	N.R.	N.R.
Silicon wafer	~ \$10	N.R.	N.R.
Piranha solution	~ \$10	N.R.	N.R.
Silane	~ \$5	N.R.	N.R.
Polycarbonate	N.R.	~ \$1	~ \$1
<b>Infrastructure</b>			
Cleanroom	Required	N.R.	N.R.
Fume hood	Required	N.R.	N.R.
Vacuum line	Required	N.R.	N.R.
Tank storage	Required	N.R.	N.R.
<b>Metrics</b>			
Equipment cost	~ \$77.5 K	~ \$16.6 K–221 K	~ \$3.15–3.85 K
Cost of new design	~ \$200–500	≤ \$6	≤ \$6
Cost of replication	~ \$15–35***	≤ \$6	≤ \$6
Min. feature size	≤ 1 μm	≥ 5 μm	75 μm
Surface roughness	1–4 nm	≥ 150 nm	≥ 200 nm
Bonding pressure	~ 350 kPa	~ 35 kPa	~ 35 kPa
Fabrication time	~ 8 h	≤ 1 h	≤ 1 h

\*N.R. Not required. \*\*P.D. Per device

\*\*\*Depending on the number of layers

## 6 Supplementary information

The supplementary information includes design files of the test devices, description of the assembly method. Also, a detailed breakdown of the fabrication cost for photolithography, high-end micromilling, and low-cost micromilling is provided. The design files are available at: <https://github.com/CIDARLAB/milling-benchmarks>.

**Acknowledgements** We like to thank Mohammadreza Rasouli from Biomat'X research laboratories at McGill University who provided a detailed pricing information on photolithography. We also like to thank Christopher Rodriguez and Sarah Nemsick for the image processing of the microfluidic droplet generation and graphic design, respectively. This work was supported by the NSF Living Computing Project Award #1522074 and NSF CAREER Award #1253856.

## References

- Aubin J, Prat L, Xuereb C, Gourdon C (2009) Effect of microchannel aspect ratio on residence time distributions and the axial dispersion coefficient. *Chem Eng Process Process Intensif* 48(1):554–559
- Ayoib A, Hashim U, Arshad MM, Thivina V (2016) Soft lithography of microfluidics channels using su-8 mould on glass substrate for low cost fabrication. In: 2016 IEEE EMBS conference on biomedical engineering and sciences (IECBES). IEEE, pp 226–229
- Bahrami M, Yovanovich M, Culham J (2006) Pressure drop of fully-developed, laminar flow in microchannels of arbitrary cross-section. *J Fluids Eng* 128(5):1036–1044
- Barbier V, Tatoulian M, Li H, Arefi-Khonsari F, Ajdari A, Tabeling P (2006) Stable modification of pdms surface properties by plasma polymerization: application to the formation of double emulsions in microfluidic systems. *Langmuir* 22(12):5230–5232



- Beebe DJ, Mensing GA, Walker GM (2002) Physics and applications of microfluidics in biology. *Ann Rev Biomed Eng* 4(1):261–286
- Brower K, White AK, Fordyce PM (2017) Multi-step variable height photolithography for valved multilayer microfluidic devices. *J Vis Exp* (119):e55276–e55276
- Chen PC, Pan CW, Lee WC, Li KM (2014) Optimization of micromilling microchannels on a polycarbonate substrate. *Int J Precis Eng Manuf* 15(1):149–154
- Dittrich PS, Schwille P (2003) An integrated microfluidic system for reaction, high-sensitivity detection, and sorting of fluorescent cells and particles. *Anal Chem* 75(21):5767–5774
- Eddings MA, Johnson MA, Gale BK (2008) Determining the optimal pdms-pdms bonding technique for microfluidic devices. *J Micro-mech Microeng* 18(6):067001
- Guckenberger DJ, de Groot TE, Wan AM, Beebe DJ, Young EW (2015) Micromilling: a method for ultra-rapid prototyping of plastic microfluidic devices. *Lab Chip* 15(11):2364–2378
- Harper CA (2000) *Modern plastics handbook: handbook*. McGraw-Hill Professional, New York
- Huang H, Densmore D (2014) Fluidic: microfluidic device synthesis for synthetic biology. *ACM J Emerg Technol Comput Syst (JETC)* 11(3):26
- Jankowski P, Ogonczyk D, Kosinski A, Lisowski W, Garstecki P (2011) Hydrophobic modification of polycarbonate for reproducible and stable formation of biocompatible microparticles. *Lab Chip* 11(4):748–752
- Kang JH, Kim YC, Park JK (2008) Analysis of pressure-driven air bubble elimination in a microfluidic device. *Lab Chip* 8(1):176–178
- Kintses B, Hein C, Mohamed MF, Fischlechner M, Courtois F, Lainé C, Hollfelder F (2012) Picoliter cell lysate assays in microfluidic droplet compartments for directed enzyme evolution. *Chem Biol* 19(8):1001–1009
- Lashkaripour A, Abouei Mehrizi A, Rasouli M, Goharimanesh M (2015) Numerical study of droplet generation process in a microfluidic flow focusing. *J Comput Appl Mech* 46(2):167–175
- Lashkaripour A, Abouei Mehrizi A, Rasouli M, Goharimanesh M, Razavi Bazaz S (2018) Size-controlled droplet generation in a microfluidic device for rare dna amplification by optimizing its effective parameters. *J Mech Med Biol* 18(1):1850002
- Lee K, Dornfeld DA (2004) A study of surface roughness in the micro-end-milling process
- Luo Y, Yu F, Zare RN (2008) Microfluidic device for immunoassays based on surface plasmon resonance imaging. *Lab Chip* 8(5):694–700
- Mian A, Driver N, Mativenga P (2011) Estimation of minimum chip thickness in micro-milling using acoustic emission. *Proc Inst Mech Eng B J Eng Manuf* 225(9):1535–1551
- Mogi K, Sugii Y, Yamamoto T, Fujii T (2014) Rapid fabrication technique of nano/microfluidic device with high mechanical stability utilizing two-step soft lithography. *Sens Actuators B Chem* 201:407–412
- Mukhopadhyay R (2007) When PDMS isn't the best. *Anal Chem* 79(9):3248–3253
- Ogonczyk D, Wegrzyn J, Jankowski P, Dabrowski B, Garstecki P (2010) Bonding of microfluidic devices fabricated in polycarbonate. *Lab Chip* 10(10):1324–1327
- Pansare VB, Sharma SB (2013) Chip load sensitive performance in micro-face milling of engineering materials. *J Braz Soc Mech Sci Eng* 35(3):285–291
- Prentner S, Allen DM, Lacombe L, Marson S, Jenkins K, Saumer M (2010) Effects of channel surface finish on blood flow in microfluidic devices. *Microsyst Technol* 16(7):1091–1096
- Rasouli M, Abouei Mehrizi A, Lashkaripour A (2015) Numerical study on low reynolds mixing oft-shaped micro-mixers with obstacles. *Transp Phenom Nano Micro Scales* 3(2):68–76
- Sackmann EK, Fulton AL, Beebe DJ (2014) The present and future role of microfluidics in biomedical research. *Nature* 507(7491):181–189
- Silva R, Bhatia S, Densmore D (2016) A reconfigurable continuous-flow fluidic routing fabric using a modular, scalable primitive. *Lab Chip* 16(14):2730–2741
- Silva R, Dow P, Dubay R, Lissandrello C, Holder J, Densmore D, Fiering J (2017) Rapid prototyping and parametric optimization of plastic acoustofluidic devices for blood-bacteria separation. *Biomed Microdevices* 19(3):70
- Solutions H (2016) *Helical machining guidebook*. Helical Solutions, LLC, Gorham
- Squires TM, Quake SR (2005) Microfluidics: fluid physics at the nanoliter scale. *Rev Mod Phys* 77(3):977
- Stone HA, Stroock AD, Ajdari A (2004) Engineering flows in small devices: microfluidics toward a lab-on-a-chip. *Annu Rev Fluid Mech* 36:381–411
- Tang J, Guo H, Zhao M, Yang J, Tsoukalas D, Zhang B, Liu J, Xue C, Zhang W (2015) Highly stretchable electrodes on wrinkled polydimethylsiloxane substrates. *Sci Rep* 5(16):527
- Thorsen T, Roberts RW, Arnold FH, Quake SR (2001) Dynamic pattern formation in a vesicle-generating microfluidic device. *Phys Rev Lett* 86(18):4163
- Tirandazi P, Hidrovo CH (2017) Liquid-in-gas droplet microfluidics; experimental characterization of droplet morphology, generation frequency, and monodispersity in a flow-focusing microfluidic device. *J Micromech Microeng* 27(7):075020
- Tsao CW, DeVoe DL (2009) Bonding of thermoplastic polymer microfluidics. *Microfluid Nanofluid* 6(1):1–16
- Ward T, Faivre M, Abkarian M, Stone HA (2005) Microfluidic flow focusing: drop size and scaling in pressure versus flow-rate-driven pumping. *Electrophoresis* 26(19):3716–3724
- Whitesides GM (2006) The origins and the future of microfluidics. *Nature* 442(7101):368–373
- Wu N, Zhu Y, Brown S, Oakeshott J, Peat T, Surjadi R, Easton C, Leech P, Sexton B (2009) A pmma microfluidic droplet platform for in vitro protein expression using crude e. coli s30 extract. *Lab Chip* 9(23):3391–3398
- Yen DP, Ando Y, Shen K (2016) A cost-effective micromilling platform for rapid prototyping of microdevices. *Technology* 4(04):234–239